PCCP

Accepted Manuscript

ROYAL SOCIETY OF CHEMISTRY

www.rsc.org/pccp

Accepted to PCCP
05/13/15

Platinum-Ruthenium Bimetallic Clusters on Graphite: A Comparison of Vapor Deposition and Electroless Deposition Methods

Randima P. Galhenage†, Kangmin Xie†, Weijian Diao††, John Meynard M. Tengco††, Grant S. Seuser †, John R. Monnier††, and Donna A. Chen†*

†Department of Chemistry and Biochemistry, University of South Carolina, Columbia, SC 29208

Phone: 803-777-1050, Fax: 803-777-9521, Email: dachen@sc.edu

††Department of Chemical Engineering, University of South Carolina, Columbia, SC 29208

Abstract:

Bimetallic Pt-Ru clusters have been grown on highly ordered pyrolytic graphite (HOPG) surfaces by vapor deposition and by electroless deposition. These studies help to bridge the materials gap between well-characterized vapor deposited clusters and electrolessly deposited clusters, which are better suited for industrial catalyst preparation. In the vapor deposition experiments, bimetallic clusters were formed by the sequential deposition of Pt on Ru or Ru on Pt. Seed clusters of the first metal were grown on HOPG surfaces that were sputtered with Ar^+ to introduce defects, which act as nucleation sites for the Pt or Ru. On the unmodified HOPG surface, both Pt and Ru clusters preferentially nucleated at the step edges, whereas on the sputtered surface, clusters with relatively uniform size and spatial distributions were formed. Low energy ion scattering experiments showed that the surface compositions of the bimetallic clusters are Pt-rich, regardless of the order of deposition, indicating that the interdiffusion of metals within the clusters is facile at room temperature. Bimetallic clusters on sputtered HOPG were prepared by the electroless deposition of Pt on Ru seed clusters from a Pt^{+2} solution using dimethylamine borane as the reducing agent at pH 11 and 40 ºC. After exposure to the electroless deposition bath, Pt was selectively deposited on Ru, as demonstrated by: the detection of Pt on the surface by XPS; and the increase in the average cluster height without an increase in the number of clusters, indicating that Pt atoms are incorporated into the Ru seed clusters.

Electroless deposition of Ru on Pt seed clusters was also achieved, but it should be noted this deposition method is extremely sensitive to the presence of other metal ions in solution that have a higher reduction potential than the metal ion targeted for deposition.

*Corresponding author

Keywords: Electroless deposition; vapor deposition; bimetallic, catalysis; scanning tunneling microscopy, X-ray photoelectron spectroscopy, low energy ion scattering,

Introduction

Electrochemical fuel cells have provided an attractive option for portable energy sources that do not rely on fossil fuels.[1-3] In particular, direct methanol fuel cells (DMFCs) have garnered substantial attention due to their high energy density, ease of handling, low operation temperature, and lack of polluting emissions.[1, 2, 4-10] A major challenge for the DMFC is the development of an anode catalyst for efficient electro-oxidation of methanol. Platinum catalysts have been used for the DMFC, and although Pt catalyzes the oxidation of methanol to CO_2, the Pt active sites become poisoned by CO.[1, 2, 6, 11-13] However, bimetallic catalysts such as Pt-Ru supported on carbon are reported to exhibit activity superior to Pt alone.[1, 2, 6, 10, 12, 14, 15] The origin of this resistance to poisoning has been explained by two well-established theories: the bifunctional mechanism and ligand effect. According to the bifunctional mechanism, the oxides of Ru provide sites for water dissociation to surface OH, which facilitates the oxidation of the intermediates of methanol decomposition that poison the active Pt sites.[16-20] The ligand (electronic) effect proposes that electronic interactions between Pt and Ru lower the energy of the d band of Pt and cause CO to bind less strongly to Pt.[15, 18, 21-25] In recent studies, the bifunctional mechanism is reported to play the dominant role, with the ligand effect providing a minor contribution to the reduced CO poisoning.[9, 14, 20]

The most active catalysts for methanol electro-oxidation are composed of highly dispersed, nanosized Pt-Ru particles deposited on a carbon support, but small variations in preparation conditions have a significant impact on activity.[1, 12] Conventional impregnation methods have difficulty controlling the dispersion and surface compositions of the Pt-Ru catalysts.[1, 2, 7, 26-29] Although colloidal and microemulsion preparation methods are known to deposit highly dispersed, nanosized Pt-Ru clusters,[28-35] these methods require complex preparation procedures and expensive starting materials, making them ill-suited for commercial scale up.[1, 2, 28, 30] Therefore, practical preparation methods that produce active Pt-Ru catalysts are still being sought. Monnier and coworkers have demonstrated that electroless deposition (ED) can be used to prepare well-dispersed, exclusively bimetallic clusters in which the two metals are well mixed.[36-42] In this method, the secondary metal in the form of a metallic salt is selectively deposited from solution on the surface of the primary metal, which has been activated by a reducing agent, rather than on the catalyst support.[37, 38, 43-45] Studies of methanol electro-oxidation with Pt-Ru catalysts on carbon (XC-72) by Weidner and coworkers show that 50% Pt-

50%Ru catalysts prepared by electroless deposition of Ru on commercial Pt/C have higher activity than the commercial bimetallic catalysts (E-TEK) of the same composition.[46] This higher activity is attributed to better mixing of Pt and Ru on the atomic scale, given that the commercial Pt-Ru catalysts are known to be poorly mixed, with particles of pure Ru and pure Pt coexisting with bimetallic particles.[47, 48]

In this work, the nucleation and growth of vapor deposited Pt, Ru and Pt-Ru clusters on highly ordered pyrolytic graphite (HOPG) are investigated and compared with bimetallic cluster growth via electroless deposition. Unlike vapor deposition, electroless deposition is a method that can be readily adapted for industrial catalyst preparation, given that electroplating has been used commercially for many years in the preparation of thin film coatings.[43] HOPG provides an atomically flat, crystalline surface to serve as a model carbon support for well-characterized bimetallic Pt-Ru clusters, and HOPG is also sufficiently conductive for STM, XPS and LEIS studies. Exclusively bimetallic clusters can be grown by either deposition of Pt on Ru (Ru+Pt) or Ru on Pt (Pt+Ru), provided that the first metal generates a high enough cluster density to serve as nucleation sites for the second metal. The HOPG surfaces are initially sputtered with Ar^+ before metal deposition to introduce defects that serve as nucleation sites. The surfaces of the bimetallic clusters are Pt-rich, regardless of the order of deposition, implying that the atoms readily diffuse within the clusters to achieve the lowest energy surface. Electroless deposition of Pt on Ru seed clusters on HOPG resulted in the formation of bimetallic clusters. Although electroless deposition of Ru on Pt was also achieved, trace Ag contamination in the $Ru(NH_3)_6Cl_3$ salt caused the deposition of Ag in addition to Ru.

Experimental

Surface characterization and preparation were carried out in an ultrahigh vacuum (UHV) chamber that has previously been described in detail.[49] This chamber has a base pressure below 1×10^{-10} Torr and is equipped with a variable-temperature STM (Omicron VT-25), a hemispherical analyzer (Omicron EA125) for X-ray photoelectron spectroscopy and low energy ion scattering experiments, and a load lock chamber for rapid introduction of new samples.

The HOPG support was purchased from SPI supplies (10 mm x 10mm x 1 mm, SPI 3). The HOPG samples were mounted on a standard Omicron tantalum sample plate and heated via electron bombardment using a tungsten filament positioned behind the sample plate.[50] Before

each experiment, a clean surface was prepared by cleaving the surface with adhesive tape in air and reintroducing the sample into the UHV chamber. Approximate temperatures were measured by a K-type thermocouple spot welded to the edge of the sample plate. In order to create surfaces with more defects for metal nucleation, the HOPG was sputtered with Ar^+ at 500 eV at a current of 0.1 μA and Ar pressure of 3 x 10^{-7} Torr for 30 seconds and 5 minutes. For comparison, the more aggressive sputtering conditions used for cleaning TiO_2(110) and Pt(111) surfaces are 1 kV, 3-5 μA, and 1-5x10^{-6} Torr for 20 min. Following sputtering, the HOPG surfaces were heated to 950-1000 K for 12 min to remove embedded Ar.

Metal deposition was achieved with an electron-beam evaporator (Oxford Applied Research, EGCO4) using a Ru bar (Good Fellow, 99.9%, 2 mm x 2 mm x 25 mm) or a Pt rod (ESPI, 99.99%, 2 mm diameter). During deposition, a +800 V bias was applied to the surface in order to repel the positively charged metal ions that are known to create defect sites for metal nucleation on HOPG.[51] Metal coverages were determined using an independently calibrated quartz crystal microbalance (Inficon, XTM-2),[52] and one monolayer (ML) is defined as the packing density of Pt(111) (1.50 x 10^{15} atoms/cm^2) or Ru(0001) (1.58 x 10^{15} atoms/cm^2).

Procedures for the electroless deposition of Pt and Ru were adapted from previous experiments conducted on Pt and Ru catalysts supported on a powdered carbon support (XC-72).[46] The general procedures for electroless deposition experiments have been described in detail elsewhere.[36, 45, 53] Concentrations of the metals in ppm are calculated from the mass of the metal only divided by the total mass of the solution. For the deposition of Pt on 0.43 ML Ru clusters on HOPG, the electroless deposition (ED) bath consisted of a 100 mL aqueous solution of 20-60 ppm Pt^{+2} (H_2PtCl_6, Sigma-Aldrich) with dimethylamine borane (DMAB, Sigma-Aldrich) as the reducing agent in a 5:1 molar ratio of DMAB:Pt^{+2}. The total deposition time in the Pt ED bath was 60 min, and an additional aliquot of DMAB was added after 30 min in order to maintain the 5:1 molar ratio, assuming that all of the initial DMAB was consumed at this time. The temperature of the ED bath was maintained at either 40 or 70 °C by immersion in a temperature-controlled water bath. The pH was fixed at 11.0 $\pm$ 0.2 through the addition of 1-2 drops of 10 M NaOH, followed by 1 M HCl and 1 M NaOH for fine adjustment, if necessary. The bath for the electroless deposition of Ru on 0.50 ML Pt clusters on HOPG was a 120 mL aqueous solution of 50 ppm Ru^{+3} ($Ru(NH_3)_6Cl_3$, Sigma-Aldrich) and formic acid (Fluka) as the reducing agent in a molar ratio of formic acid:Ru^{+3} of 10:1. The total deposition time in the Ru

ED bath was 90 min, and additional aliquots of formic acid solution were added after 30 and 60 min to maintain the 10:1 molar ratio. The temperature of the bath was set at 90 °C, and a pH of 3.5-4 was maintained through the addition of HCl and NaOH. After removal of the HOPG sample from the ED bath, the surface was thoroughly washed with deionized water before transferring into the UHV chamber for surface analysis. All aqueous solutions were prepared with deionized water, experiments were carried out in single-use polypropylene cups, and the ED baths were vigorously stirred during deposition.

STM experiments for clusters on HOPG were carried out with a constant tunneling current of 0.1-0.2 nA and a sample bias of +2-2.3 V with respect to the tip; the clean HOPG surface was imaged with a 0.8 nA tunneling current and +1.0 V bias. STM tips consisted of 0.38 mm diameter tungsten wire that was electrochemically etched in NaOH and conditioned by voltage pulsing and sputtering with Ar^+.[54] Cluster heights are reported as a measure of cluster size since tip convolution effects are known to significantly overestimate diameters.[52, 54-56] The average cluster heights and standard deviations were determined using an in-house program[57, 58] that measured all clusters in a 100 x 100 nm^2 image. For the following surfaces, 50 clusters were measured manually because the program was unable to accurately assess the heights of clusters: 0.50 ML of Pt and 0.43 ML of Ru on unmodified HOPG, and 0.43 ML Ru+Pt ED (20, 50 ppm Pt^{+2}).

LEIS experiments were carried out with a 600 eV He^+ beam using a dwell time of 0.1 s, step size of 0.2 eV and a current to the sample of 25 μA. Exposure to the ion beam was minimized to prevent damage to the surface during the LEIS experiment. XPS studies were conducted with an AlKα anode (1486.6 eV) using a dwell time of 0.2 s and step size of 0.02 eV.

Results

An STM image of the freshly cleaved HOPG surface shows that the surface consists of atomically flat terraces that are as wide as 1000 Å. The terraces are separated steps of 5-10 Å in height, which correspond ~1-3 atomic layers (Figure 1a). When 0.25 ML of Pt is deposited on this freshly cleaved surface, three-dimensional clusters are formed with a cluster density of 0.12 x 10^{12} cm^{-2}, and these clusters are preferentially found at the step edges, which are the favored coordination sites (Figure 1b). The average height for the clusters at the step edge is 33.0 $\pm$ 3.7 Å while the larger clusters on the terraces have heights ranging from 40-50 Å. Furthermore, it

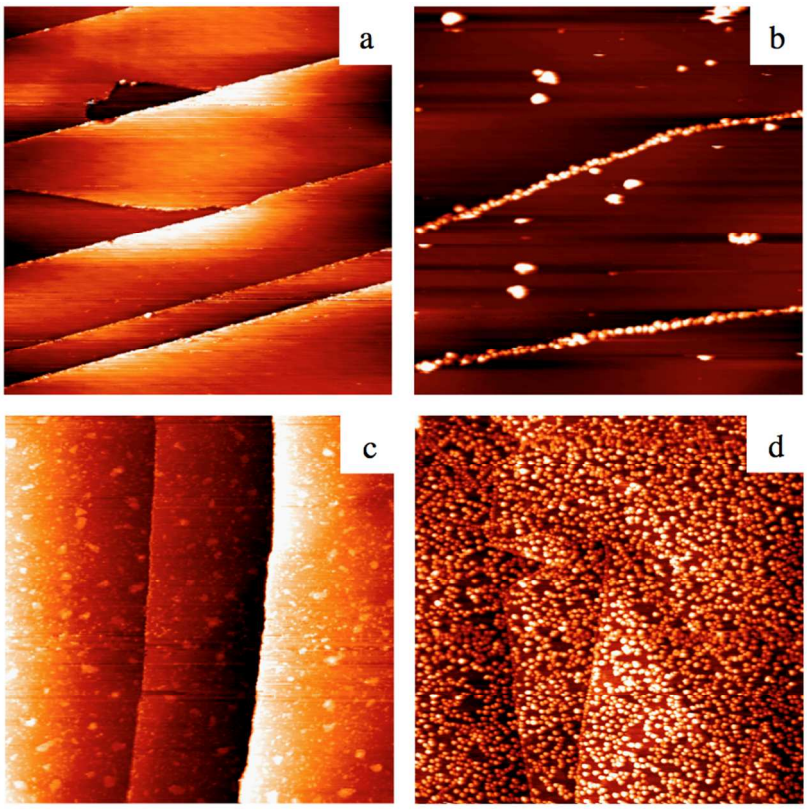

Figure 1: Scanning tunneling microscopy images of: a) a freshly cleaved HOPG surface; b) 0.25 ML Pt on HOPG; c) modified HOPG (m-HOPG) prepared by Ar^+ sputtering for 30 s; and d) 0.25 ML Pt on m-HOPG. All images are 4000 Å x 4000 Å.

was difficult to collect high quality images due to the relatively strong interactions between the Pt clusters and the STM tip. These interactions are a consequence of the weak binding between Pt and the HOPG support,[59] and the fact that the glitches often coincide with the appearance of fully or partially imaged Pt clusters on the terraces suggests that the clusters are picked up or dropped by the STM tip. The presence of the majority of the Pt clusters at the steps implies that Pt atoms are mobile on the surface at room temperature and diffuse to the preferred step sites; alternatively, it is possible that the STM tip sweeps the clusters across the terraces to the step edges.

In order to systematically study nucleation and growth of bimetallic clusters via sequential deposition, a more uniform cluster density over the surface is desirable. Therefore, the HOPG surface was sputtered with Ar^+ to intentionally create surface defects that serve as nucleation sites. After sputtering at 500 eV for 30 s with a 0.1 μA current to the sample, the resulting STM image of the clean HOPG shows that the surface has become more heterogeneous with defect sites appearing on the terraces (Figure 1c); this treatment creates the modified HOPG (m-HOPG) surface. In contrast to growth on the unmodified surface, an STM image of 0.25 ML of Pt

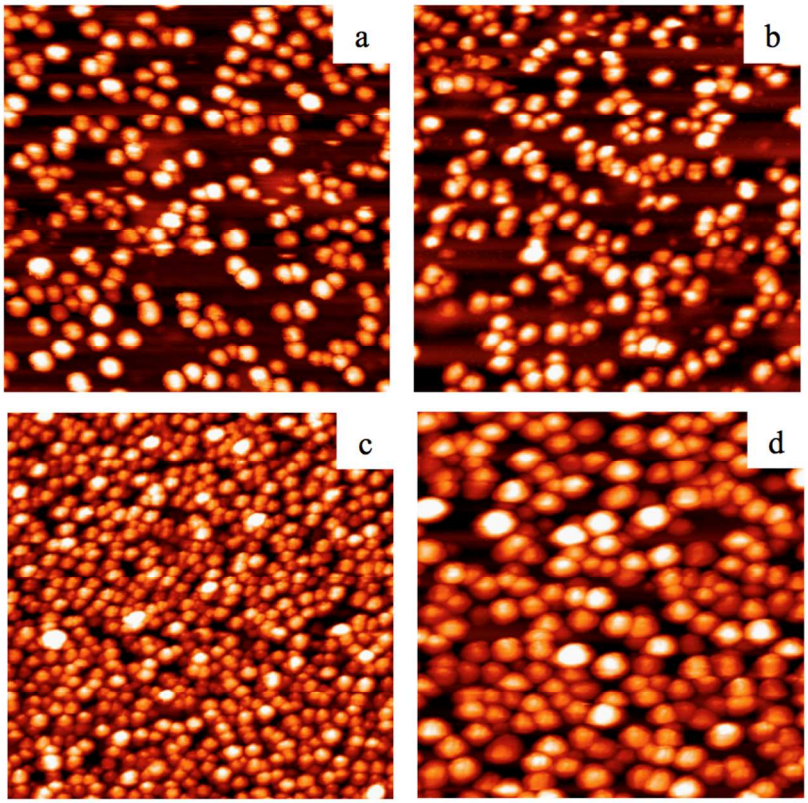

Figure 2: Scanning tunneling microscopy images of: a) 0.25 ML Pt on m-HOPG (sputtered 30 s); b) 0.50 ML Pt on m-HOPG; c) 0.50 ML Pt on hm-HOPG (sputtered 5 min); and d) 0.50 ML Pt + 0.43 ML Ru on m-HOPG. All images are 1000 Å x 1000 Å.

deposited on m-HOPG shows that the nucleation density increases by a factor of ~20 (2.25 x 10^{12} cm^{-2}), the average cluster height decreases to 14.6 ± 2.7 Å, and clusters are nucleated uniformly over the surface (Figure 1d). Average cluster heights and densities for various surfaces are summarized in Table 1. These results are consistent with previous studies reporting that Ar^+ ion sputtering selectively creates nucleation sites for metals on HOPG.[51, 60-65]

A comparison of 0.25 ML and 0.50 ML of Pt on m-HOPG for smaller 1000 Å x 1000 Å images is presented in Figures 2a and b. The cluster density for 0.50 ML of Pt (2.68 x 10^{12} cm^{-2}) is nearly the same as for 0.25 ML, but the average cluster height increases to 16.0 $\pm$ 3.5 Å, implying that the additional Pt atoms contribute to larger cluster sizes rather than nucleating new clusters. Therefore, it appears that almost all of the nucleation sites already are occupied by Pt clusters at a coverage of 0.25 ML. When the HOPG support was sputtered for 5 min to create additional nucleation sites, the deposition of 0.50 ML of Pt on this highly modified surface (hm-HOPG) resulted in the smallest clusters (11.3 $\pm$ 2.7Å) with the highest nucleation density (6.69 x 10^{12} cm^{-2}) (Figure 2c).

Bimetallic Pt-Ru clusters are prepared by depositing 0.43 ML of Ru on the 0.50 ML Pt clusters (Pt+Ru) on m-HOPG. A comparison of Figures 2b and 2d indicates that the addition of

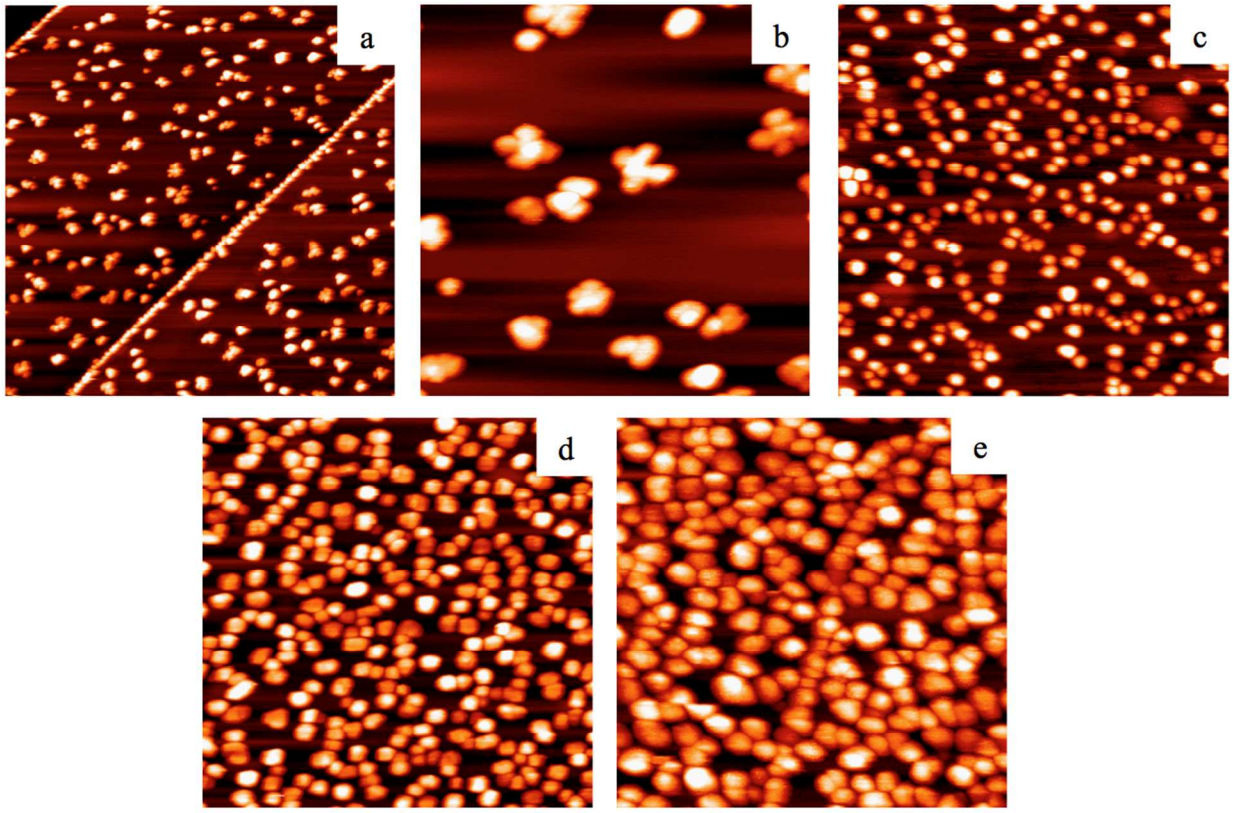

Figure 3: Scanning tunneling microscopy images of: 0.22 ML Ru on unmodified HOPG: a) 4000 Åx4000 Å and b) 1000 Å x 1000 Å; c) 0.22 ML Ru on modified HOPG; d) 0.43 ML Ru on m-HOPG; and e) 0.43 ML Ru + 0.50 ML Pt on m-HOPG. Images c-e are 1000 Å x1000 Å.

0.43 ML of Ru caused a *decrease* in cluster density from 2.68 to 2.46 x 10^{12} cm^{-2} due to cluster coalescence at the higher coverage, while the average cluster size increased from 16.0 $\pm$ 3.5 Å to 22.8 $\pm$ 6.0 Å. Thus, exclusively bimetallic clusters are formed, given that the incoming Ru atoms nucleate at the existing Pt clusters instead of forming new clusters of pure Ru. Histograms of the cluster heights for all of the clusters imaged over a 1000 Å ×1000 Å region on m-HOPG are presented in Supplemental Figure 1. These histograms demonstrate that the cluster heights increase with increasing coverage, and the addition of the second metal results in a shift in the size distribution toward higher values.

The growth of pure Ru clusters on HOPG was also investigated in order to understand the formation of bimetallic clusters via the sequential deposition of Pt on Ru. The deposition of 0.22 ML of Ru on the unmodified HOPG surface (Figure 3a,b) demonstrates that the relatively high mobility of the Ru atoms allows the Ru clusters to fill all of the sites at the step edges. However, two thirds of the clusters also reside on the terraces, in contrast to the behavior of Pt on

unmodified HOPG; this implies that the interaction of the metal clusters with HOPG is weaker in the case of Pt. The average height of clusters on the terraces is 15.8 ± 3.0 Å while the density of all clusters is 0.19 x 10^{12} cm^{-2}, which is 1.6 times higher than for Pt on HOPG. In general, the clusters at the steps are slightly larger (18.7 ± 2.0 Å) than at the terraces. Furthermore, the Ru clusters do not have symmetrical shapes but instead exist as clusters of smaller particles.

After modifying the HOPG surface by sputtering for 30 s (m-HOPG), the deposition of 0.22 ML of Ru results in smaller clusters with an average height of 11.7 ± 2.3 Å and a higher cluster density of 2.95 x 10^{12} cm^{-2} (Table 1, Figure 3c). Increasing the Ru coverage to 0.43 ML m-HOPG produces larger clusters (17.3 ± 2.9 Å), while the cluster density increases by only ~10% compared to the 0.22 ML coverage (3.28 x 10^{12} cm^{-2}, Figure 3d). Both these values are similar to those of 0.50 ML of Pt on m-HOPG, with heights within 10% and cluster densities within 20%. Furthermore, the Ru clusters have more distinctly facetted shapes than Pt, suggesting that the Pt atoms are more mobile within the clusters than Ru such that the Pt atoms are not locked into specific configurations at room temperature.

After the deposition of 0.50 ML of Pt on the 0.43 ML Ru clusters (Ru+Pt), the cluster density decreases to 2.82 x 10^{12} cm^{-2} as a result of cluster coalescence, and the average cluster height increases to 19.4 ± 3.9 Å (Figure 3e). The larger cluster heights and lower cluster density imply that Pt atoms nucleate at Ru clusters to grow bimetallic clusters, rather than forming new nucleation sites for pure Pt clusters. Notably, the cluster heights and densities are similar for the two bimetallic surfaces although the Pt+Ru surface has a larger average cluster height and lower density due to the initially higher cluster density for pure Ru compared to pure Pt.

LEIS experiments were carried out to evaluate the surface compositions of the Pt+Ru and Ru+Pt bimetallic clusters (Figure 4). In order to calculate the surface compositions based on the integrated LEIS peaks, the relative sensitivity factors for Pt and Ru were determined by growing 5 ML Ru and 5 ML Pt films on a Pt foil substrate. At this coverage, LEIS experiments showed that the Ru completely covers the Pt foil, given that no Pt signal is detected. The sensitivity for detection of Pt was found to be 1.74 times greater than for Ru, assuming identical surface areas for the films. The surfaces of 0.50 ML Pt+0.43 ML Ru clusters were 80% Pt, whereas the 0.43 ML Ru+0.50 ML Pt clusters were 93% Pt. Furthermore, when the clusters were heated to 130 °C for 3 min, the surface compositions increased to 98-99% Pt for both surfaces. Thus, the

bimetallic clusters are rich in Pt regardless of the order of deposition and reach ~100% Pt when

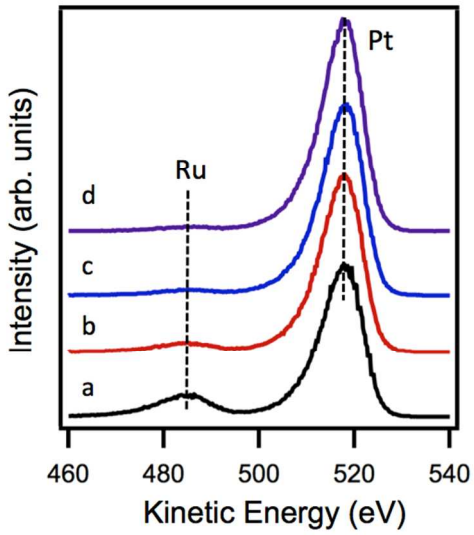

Figure 4. Low energy ion scattering data for the following clusters on m-HOPG: a) 0.50 ML Pt+0.43 ML Ru; b) 0.50 ML Pt+0.43 ML Ru heated to 130 °C for 3 min; c) 0.43 ML Ru+0.50 ML Pt; and d) 0.43 ML Ru+0.50 ML Pt heated to 130 °C for 3 min.

the clusters are heated to achieve equilibrium. These results are consistent with the higher surface free energy for Ru (~2.7 J/m^2) compared to Pt (~2.2 J/m^2), which favors Pt at the surface.[66]

Figures 5 and 6 show STM and Pt(4f) XPS data for the electroless deposition of Pt on 0.43 ML Ru clusters on m-HOPG under various conditions (see experimental section for details). No Pt deposition occurs when the freshly cleaved HOPG substrate itself is exposed to the Pt ED bath. All of the surfaces exposed to the ED baths are heated to ~130 °C for 3 min before STM and XPS analysis in order to remove surface contamination that prevents imaging by STM. Since the metal clusters increase in size after heating to 130 °C, the ED experiments are compared with vapor deposition experiments in which the surfaces have also been heated to 130 °C. For example, when the vapor deposited 0.43 ML Ru+0.50 ML Pt clusters are heated to 130 °C, a 50% decrease in cluster density is accompanied by a ~15% increase in cluster height (Supplemental Figure 1, Table 1).

In the first Pt ED experiment with 50 ppm Pt^{+2} at 70 °C, the STM image demonstrates that the surface consists of large clusters with heights ranging from 15 to 65 Å (34.5 ± 10.9 Å) and a cluster density of 1.66 x 10^{12} cm^{-2} (Figure 5a). The Pt(4f) region in the XPS data for this surface confirms that Pt was deposited; based on a comparison of the Pt(4f) intensity with that of vapor deposited 0.43 ML Ru+0.50 ML Pt, the Pt coverage in the ED experiment is well over 0.5 ML (Figure 6). Due to the high coverage of Pt, it is not possible to determine if Pt deposits selectivity on the Ru seed clusters. Therefore, in the second ED experiment, the Pt^{+2}

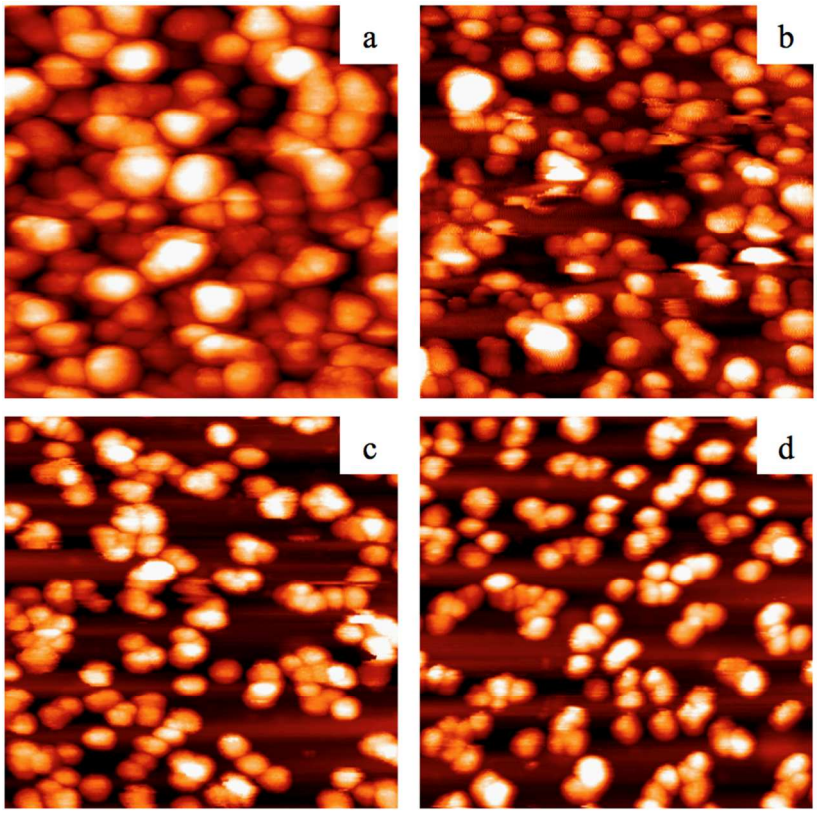

Figure 5. Scanning tunneling microscopy images for 0.43 ML Ru on m-HOPG after: a) electroless deposition of Pt (50 ppm of Pt^{+2} at 70° C); b) electroless deposition of Pt (20 ppm of Pt^{+2} at 70° C); c) electroless deposition of Pt (60 ppm of Pt^{+2} at 40° C); and d) exposure to the same electroless deposition conditions in (c) without Pt^{+2}. All surfaces were heated to 130 °C for 3 min, and images are 1000 Å x 1000 Å.

concentration was decreased to 20 ppm, which resulted in a Pt coverage below 0.5 ML (Figure 6). The STM image of this surface (Figure 5b) shows clusters with nonuniform heights ranging from 10 to 60 Å (24.0 ± 5.9 Å average height, cluster density of 1.95 x 10^{12} cm^{-2}), and the surface is difficult to image without the tip crashing on the very large clusters. In the third ED experiment, the temperature was reduced to 40 °C in order to decrease the rate of Pt deposition

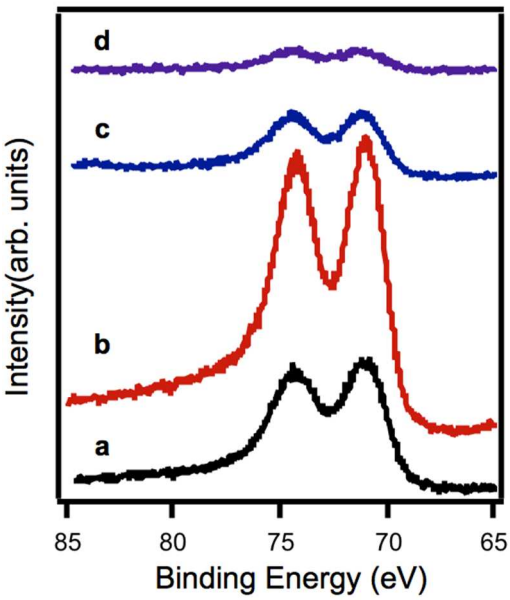

Figure 6. X-ray photoelectron spectroscopy data for the Pt(4f) region for 0.43 ML Ru on m-HOPG after the following treatments: a) vapor deposition of 0.50 ML Pt; b) Pt electroless deposition (50 ppm, 70 °C); c) Pt electroless deposition (20 ppm, 70 °C); and d) Pt electroless deposition (60 ppm, 40 °C). All of the surfaces exposed to the ED baths (b-d) were annealed at 130 °C for 3 min.

and promote more uniform cluster growth. At a Pt^{+2} concentration of 20 ppm, no Pt was detected by XPS, but a small amount of Pt was deposited from a 60 ppm Pt^{+2} solution at the same temperature (Figure 6); this coverage is estimated to be less than 0.1 ML based on the integrated Pt intensity compared to that of the vapor-deposited 0.43 ML Ru+0.50 ML Pt clusters. An STM image of this surface shows clusters with an average height of 22.8 $\pm$ 4.6 Å and a cluster density of 1.53 x 10^{12} cm^{-2} (Figure 5c). In order to understand changes due to cluster sintering in the ED bath, 0.43 ML of Ru on m-HOPG was exposed to ED conditions in the absence of the Pt^{+2} salt. XPS data from the resulting surface indicated that no Pt was deposited, and the Ru clusters had an average height of 19.9 $\pm$ 4.7 Å with a cluster density of 1.58 x 10^{12} cm^{-2}. The nearly identical cluster densities and larger cluster sizes for the third Pt ED experiment compared to this surface demonstrate that bimetallic clusters are formed via selective deposition of Pt at the Ru seed clusters. The cluster size distributions for these two surfaces confirm that there is a shift to larger sizes after ED of Pt (Supplemental Figure 1).

XPS data for the Ru(3d) region are presented in Figure 7, with the Ru($3d_{5/2}$) peak at 280 eV and the Ru($3d_{3/2}$) and C(1s) peaks contributing to the feature at ~284.3 eV. For comparison to the ED experiments, the spectrum of vapor deposited 0.43 ML Ru+0.50 ML Pt appears at the bottom of the figure. The Ru ($3d_{5/2}$) peak is observed for all experiments, indicating that Ru remains on the surface in the ED process. As expected, the intensity of the Ru($3d_{5/2}$) peak decreases with increasing Pt coverage and is attenuated to 40-60% of the intensity of vapor deposited 0.43 ML Ru clusters. Notably, the 0.43 ML Ru clusters exposed to the ED bath

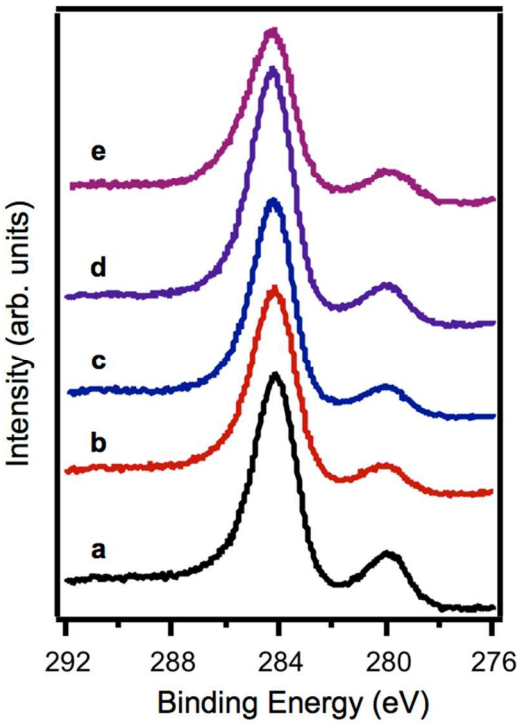

Figure 7. X-ray photoelectron spectroscopy data for the Ru(3d)/C(1s) region for 0.43 ML Ru on m-HOPG after the following treatments: a) vapor deposition of 0.50 ML Pt; b) Pt electroless deposition (50 ppm, 70 °C); c) Pt electroless deposition (20 ppm, 70 °C); d) Pt electroless deposition (60 ppm, 40 °C); and e) exposure to the ED bath in (d) without Pt^{+2}. All of the surfaces exposed to the ED baths (b-e) were annealed at 130 °C for 3 min.

without Pt^{+2} also exhibit a 40% decrease in Ru intensity compared to the freshly deposited 0.43 ML Ru clusters due to contamination of the Ru surface upon exposure to air.

Electroless deposition of Ru on Pt seed clusters on hm-HOPG was carried out for 0.50 ML Pt clusters in an ED bath consisting of 50 ppm Ru^{+3} and formic acid (formic acid:Ru^{+3}=10:1) as the reducing agent at a pH of 3.5-4 and temperature of 90 °C; the hm-HOPG was used to create more nucleation sites for Ru deposition and ensure a detectable Ru XPS signal. The appearance of a Ru($3d_{5/2}$) peak indicates that Ru was deposited on the surface, and the Pt(4f) spectrum after deposition shows that Pt remains on the surface after Ru ED (Figure 8). However, Ag deposition is also detected by XPS, and inductively coupled plasma emission spectroscopy experiments confirm that there is trace Ag contamination in the $Ru(NH_3)_6Cl_3$ solution. Based on the relative XPS sensitivities for Ag($3d_{5/2}$) and Ru ($3d_{5/2}$),[67] the amounts of Ag and Ru deposited are estimated to be roughly the same. LEIS experiments also establish the presence of Ag on the surface. Given that Ag^+ is much more easily reduced than Ru^{+3} based on their relative electrochemical reduction potentials, the concentration of Ag^+ in solution can be extremely low and still result in significant Ag deposition compared to Ru. Furthermore, the relatively small number of surface sites on the vapor-deposited Pt clusters results in comparable coverages of Ru and Ag because the Ag contaminant is preferentially deposited on the clusters before Ru deposition can occur. Ru ED could not be carried out with other Ru salts because either Ru^{+n}

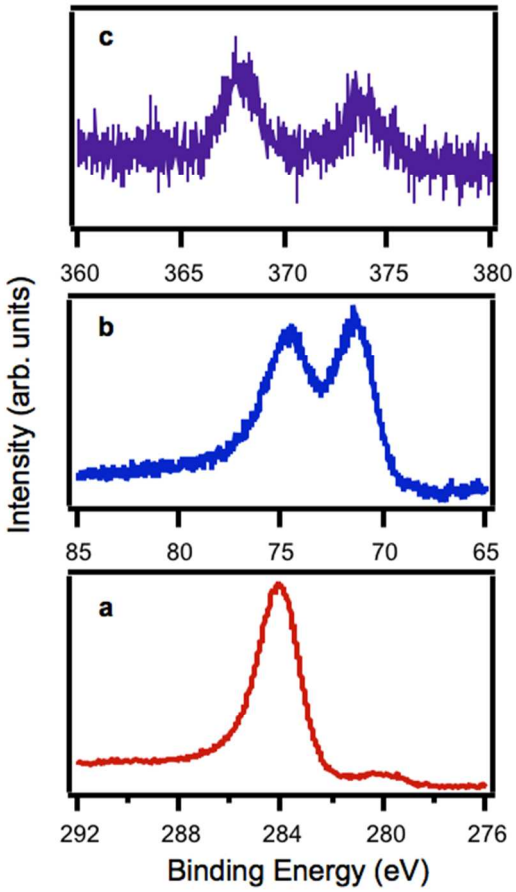

Figure 8. X-ray photoelectron spectroscopy data for the: a) Ru(3d)/C(1s); b) Pt(4f); and c) Ag(3d) regions for 0.50 ML Pt on hm-HOPG after exposure to the Ru ED bath. The surface was annealed at 130 °C for 3 min.

was unstable in solution under ED conditions (K_2RuCl_5, $RuCl_3$, $Ru(NH_3)_6Cl_2$), or the solution was too thermally stable for the reduction of Ru^{+n} ($K_4Ru(CN)_6$). All attempts to selectively remove the Ag^+ contamination from the Ru^{+3} solution were not successful (see Supplemental text 1).

Discussion

On the unmodified HOPG surface, weak Pt substrate interactions result in high mobility of the Pt atoms and nearly exclusive nucleation of clusters at the step edges. The small fraction of clusters appearing on the terraces is likely due to interactions between the STM tip and Pt clusters that cause cluster displacement. Similarly, other studies of metal clusters such as Pt,[59] Ru[51] and Ag[12, 68, 69] on freshly cleaved HOPG have also shown that weak cluster-support interactions coupled with stronger cluster-tip interactions lead to the tip-induced movement of the clusters on the surface. In general, the mobility of metal atoms on the unmodified HOPG surface is high at room temperature, and consequently the metal clusters are often found at the

favored low-coordinated step sites.[61 , 63, 69 , 70, 71] However, Ru atoms interact more strongly with HOPG and have decreased mobility, as demonstrated by the higher fraction of Ru clusters found on the terraces and the 60% higher cluster density compared to Pt. Furthermore, the Ru clusters exist on unmodified HOPG as aggregates of smaller particles, and the lack of coalescence of the smaller particles is attributed to different rotational orientations of the crystalline particles with respect to the surface, given that stacking faults preventing coalescence can be formed when particles of two different orientations grow together. In fact, Ru is reported to grow epitaxially on modified HOPG surfaces with two different growth orientations.[72] In both cases, the (0001) face of Ru is parallel to the graphite surface, but one orientation is the same as the graphite lattice whereas the other is rotated by 30°. The aggregates of particles are not observed on m-HOPG, where the Ru clusters have nearly facetted shaped. However, the sizes of the clusters on m-HOPG are generally smaller than the uncoalesced particles on unmodified HOPG due to the shorter Ru diffusion lengths on the more defective m-HOPG.

The nucleation densities of Pt and Ru clusters on HOPG are controlled by creating nucleation sites via Ar^+ ion sputtering. For the same metal coverages, a more highly sputtered surface results in a higher cluster density as well as smaller cluster sizes, and the clusters have a relatively narrow size distribution. Even after sputtering to introduce nucleation sites, the number of clusters for Ru is higher than for Pt, and this is attributed to the higher mobility of Pt atoms on the surface and weaker metal-HOPG interaction for Pt. Furthermore, the difference in cluster densities is greater on the unmodified surface; the Ru density is ~60% higher on the unmodified surface but only 20-30% higher on m-HOPG for metal coverages of 0.22-0.43 ML. Other literature studies also shown that metal particles with uniform size and spatial distributions are observed after defect sites have been intentionally introduced to the HOPG surface either by sputtering with an inert gas,[51, 60-65] or by sputtering followed by oxidation in air at temperatures above 500 °C.[12, 60, 68, 72]

Bimetallic clusters are formed from sequential vapor deposition of Ru on Pt or Pt on Ru for 0.4-0.5 ML coverages of both metals on m-HOPG. For bimetallic clusters growth on TiO_2(110), our group has shown that exclusively bimetallic clusters can be grown when the less mobile metal is deposited first, followed by the more mobile metal.[52, 54, 57, 73-75] Moreover, it is also possible to form only bimetallic clusters through either order of sequential deposition as long as the number of nucleation sites formed during the deposition of the first metal exceeds the

number of nucleation sites required during the deposition of the second metal.[75] In the case of Pt and Ru on m-HOPG, a 0.4-0.5 ML coverage of either metal provides the requisite number of nucleation sites for the 0.4-0.5 ML coverage of the second metal. Furthermore, on m-HOPG the diffusion length is controlled primarily by the number of defect sites induced by sputtering rather than by the intrinsic mobility of the metals. The surface compositions of the bimetallic clusters are close to 100% Pt after heating to 130 °C, and this is consistent with predictions from bulk thermodynamics, given that Pt has a lower surface free energy than Ru (2.2 J/m^2 vs. 2.7 J/m^2).[66] At room temperature, the deposition of Ru on Pt results in cluster surfaces that are only 80% Pt because the atoms have insufficient energy to diffuse within the clusters and achieve the equilibrium surface compositions. However, even at room temperature the diffusion of atoms within a cluster is facile enough to reach an 80% Pt surface composition for Ru deposited on Pt. Although the cluster sizes and densities are similar for the Pt+Ru and Ru+Pt surfaces, the Ru+Pt surface has a slightly smaller average cluster height (19.4 $\pm$ 3.9 Å vs. 22.8 $\pm$ 6.0 Å) and a 15% higher cluster density because the initial deposition of the Ru seed clusters provides more nucleation sites than the deposition of Pt seed clusters. Previous LEIS studies of Pt-Ru films on HOPG also report a strong tendency for surface segregation of Pt; deposition of 30 Å of Ru on 50 Å of Pt resulted in both Pt and Ru at the surface, whereas 30 Å of Pt on 50 Å of Ru resulted in a pure Pt surface.[76] In addition, encapsulation of Ru and Pt by carbon from the support was observed for 50 Å films deposited on HOPG after heating to 700 °C,[77] but no such cluster encapsulation was observed at the lower temperature of 130 °C in this study.

Similar bimetallic Pt-Ru clusters are also grown on m-HOPG using the technique of electroless deposition, which bridges the materials gap between vapor-deposited clusters on model surfaces and the electroless deposition method that can be extended to industrial catalyst preparation. Specifically, Pt is deposited from solution onto Ru seed clusters supported on m-HOPG. To our knowledge, this is the first instance in which bimetallic clusters have been grown by electroless deposition and characterized on an atomically flat model support such as graphite. The bimetallic cluster densities are nearly identical to that of the monometallic seed clusters exposed to the ED without Pt^{+2} and heated to 130 °C, while the average cluster heights increase, and the deposition of Pt is confirmed by XPS. The amount of Pt deposited can be controlled by changing the Pt^{+2} concentration in the ED bath, and the rate of metal deposition can be decreased to form more uniformly-sized clusters by decreasing the temperature of the ED bath. Although

Ru deposition on Pt seed clusters could be achieved by electroless deposition, the presence of a Ag contaminant in the $Ru(NH_3)_6Cl_3$ salt results in the codeposition of Ag. It should also be noted that electroless deposition is extremely sensitive to trace contaminants of other metals, particularly if the reduction potential for the contaminant metal is significantly higher, as is the case for Ag and Ru. A Ag contamination level of only 2.5×10^{-5} g Ag/g Ru provides enough Ag atoms to completely cover the 0.50 ML Pt clusters on m-HOPG in the Ru^{+3} ED experiment because these model surfaces have a relatively small number of surface sites compared to conventional catalysts on powdered supports (see Supplemental text 2).

Conclusions

Bimetallic Pt-Ru clusters have been grown on HOPG via vapor deposition in UHV and electroless deposition in solution. In contrast to cluster growth via vapor deposition in vacuum, the technique of electroless deposition is one that is suitable for commercial catalyst preparation, given that electroplating is already widely used in industry. Thus, the ability to grow bimetallic clusters on model, atomically flat surfaces by electroless deposition allows the materials gap to be bridged between fundamental investigations of clusters grown on single-crystal support surfaces and studies of industrial catalysts. The first step in the growth of bimetallic clusters is the deposition of seed clusters of pure Ru or Pt, which serve as nucleation sites for the deposition of the second metal; the higher mobility of Pt on HOPG compared to Ru is attributed to weaker metal-HOPG interactions for Pt. The number of seed clusters on HOPG can be controlled by Ar^+ sputtering, which creates defects that serve as nucleation sites. For the same metal coverages, the cluster density increases with Ar^+ sputtering time, and the average cluster height decreases. Bimetallic clusters can be grown through sequential vapor deposition of either Pt on Ru (Ru+Pt) or Ru on Pt (Pt+Ru), provided that the initial deposition creates a sufficient number of seed clusters for the nucleation of the second metal. The fact that the resulting cluster surfaces are nearly 100% Pt after heating to 130 °C for both orders of deposition demonstrates that diffusion of metal atoms within the clusters occurs readily at this temperature and is consistent with the lower surface free energy of Pt compared to Ru. Electroless deposition of Pt on Ru seed clusters was achieved using $PtCl_6^{-2}$ with DMAB as a reducing agent, and STM images of the resulting surface indicate that the Pt deposition occurred only at the Ru seed clusters. The electroless deposition of Ru on Pt seed clusters was also carried out from a solution of

$Ru(NH_3)_6Cl_3$ with formic acid as a reducing agent; these experiments show that electroless deposition is exceptionally sensitive to trace contaminants of metal ions with a higher reduction potential than the metal ion targeted for deposition, given that extremely low concentrations of Ag^+ in the Ru salt solution resulted in the deposition of both Ag and Ru.

Acknowledgements

We gratefully acknowledge financial support from University of South Carolina's Office of Research (ASPIRE II grant) and from the National Science Foundation (CHE 1300227).

Table 1. Average cluster heights and cluster densities for metals on HOPG. All of the surfaces exposed to the Pt ED bath were heated to 130 °C.

Surface	Average Cluster Height (Å)	Cluster Density ($x10^{12}/cm^2$)
0.25 ML Pt/HOPG	33.0±3.7	0.12
0.25 ML Pt/m-HOPG	14.6±2.7	2.25
0.50 ML Pt/m-HOPG	16.0±3.5	2.68
0.50 ML Pt/hm-HOPG	11.3±2.7	6.69
0.50 ML Pt+0.43 ML Ru/m-HOPG	22.8±6.0	2.46
0.22 ML Ru/HOPG	15.8±3.0	0.19
0.22 ML Ru/m-HOPG	11.7±2.3	2.95
0.43 ML Ru/m-HOPG	17.3±2.9	3.28
0.43 ML Ru+0.50 ML Pt/m-HOPG	19.4±3.9	2.82
0.43 ML Ru+0.50 ML Pt/m-HOPG, 130 °C	22.5±4.7	1.36
0.43 ML Ru+Pt ED (50 ppm Pt^{+2}, 70° C)	34.5±10.9	1.66
0.43 ML Ru+Pt ED (20 ppm Pt^{+2}, 70° C)	24.0±5.9	1.95
0.43 ML Ru+Pt ED (60 ppm Pt^{+2}, 40° C)	22.8±4.6	1.53
0.43 ML Ru+ED bath 40° C, no Pt^{+2}	19.9±4.7	1.58

References

1. H. S. Liu, C. J. Song, L. Zhang, J. J. Zhang, H. J. Wang and D. P. Wilkinson, *J. Power Sources*, 2006, **155**, 95.
2. A. S. Arico, S. Srinivasan and V. Antonucci, *Fuel Cells*, 2001, **1**, 133.
3. A. K. Shukla, A. S. Arico and V. Antonucci, *Renew. Sust. Energ. Rev.*, 2001, **5**, 137.
4. N. M. Markovic and P. N. Ross, *Electrochim. Acta*, 2000, **45**, 4101.
5. R. Dillon, S. Srinivasan, A. S. Arico and V. Antonucci, *J. Power Sources*, 2004, **127**, 112.
6. J. M. Leger, S. Rousseau, C. Coutanceau, F. Hahn and C. Lamy, *Electrochim. Acta*, 2005, **50**, 5118.
7. E. Antolini, *Mater. Chem. Phys.*, 2003, **78**, 563.
8. B. D. McNicol, D. A. J. Rand and K. R. Williams, *J. Power Sources*, 1999, **83**, 15.
9. S. Wasmus and A. Kuver, *J. Electroanal. Chem.*, 1999, **461**, 14.
10. C. Lamy, J. M. Leger and S. Srinivasan, in *Modern Aspects of Electrochemistry*, eds. O. M. Bockris, B. E. Conway and R. E. White, Plenum Press, New York, 2000, vol. 34, pp. 53.
11. R. Parsons and T. Vandernoot, *J. Electroanal. Chem.*, 1988, **257**, 9.
12. C. Roth, A. J. Papworth, I. Hussain, R. J. Nichols and D. J. Schiffrin, *J. Electroanal. Chem.*, 2005, **581**, 79.
13. A. Kabbabi, R. Faure, R. Durand, B. Beden, F. Hahn, J. M. Leger and C. Lamy, *J. Electroanal. Chem.*, 1998, **444**, 41.
14. T. Frelink, W. Visscher and J. A. R. Vanveen, *Surf. Sci.*, 1995, **335**, 353.
15. K. Sasaki, J. X. Wang, M. Balasubramanian, J. McBreen, F. Uribe and R. R. Adzic, *Electrochim. Acta*, 2004, **49**, 3873.
16. M. Watanabe and S. Motoo, *J. Electroanal. Chem.*, 1975, **60**, 267.
17. S. L. Gojkovic, T. R. Vidakovic and D. R. Durovic, *Electrochim. Acta*, 2003, **48**, 3607.
18. P. Waszczuk, G. Q. Lu, A. Wieckowski, C. Lu, C. Rice and R. I. Masel, *Electrochim. Acta*, 2002, **47**, 3637.
19. N. M. Markovic, H. A. Gasteiger, P. N. Ross, X. D. Jiang, I. Villegas and M. J. Weaver, *Electrochim. Acta*, 1995, **40**, 91.
20. C. Lu and R. I. Masel, *J. Phys. Chem. B*, 2001, **105**, 9793.
21. P. Liu and J. K. Norskov, *Fuel Cells*, 2001, **1**, 192.
22. F. B. de Mongeot, M. Scherer, B. Gleich, E. Kopatzki and R. J. Behm, *Surf. Sci.*, 1998, **411**, 249.
23. H. Igarashi, T. Fujino, Y. M. Zhu, H. Uchida and M. Watanabe, *Phys. Chem. Chem. Phys.*, 2001, **3**, 306.
24. E. Christoffersen, P. Liu, A. Ruban, H. L. Skriver and J. K. Norskov, *J. Catal.*, 2001, **199**, 123.
25. H. Rauscher, T. Hager, T. Diemant, H. Hoster, F. B. De Mongeot and R. J. Behm, *Surf. Sci.*, 2007, **601**, 4608.
26. J. H. Sinfelt, *Bimetallic Catalysts. Discoveries, Concepts, and Applications*, John Wiley and Sons, New York, 1983.
27. M. Gotz and H. Wendt, *Electrochim. Acta*, 1998, **43**, 3637.
28. Z. L. Liu, X. Y. Ling, X. D. Su and J. Y. Lee, *J. Phys. Chem. B*, 2004, **108**, 8234.

29. T. J. Schmidt, M. Noeske, H. A. Gasteiger, R. J. Behm, P. Britz and H. Bonnemann, *J. Electrochem. Soc.*, 1998, **145**, 925.
30. Z. L. Liu, J. Y. Lee, M. Han, W. X. Chen and L. M. Gan, *J. Mat. Chem.*, 2002, **12**, 2453.
31. Z. L. Liu, J. Y. Lee, W. X. Chen, M. Han and L. M. Gan, *Langmuir*, 2004, **20**, 181.
32. H. Bonnemann, R. Brinkmann, P. Britz, U. Endruschat, R. Mortel, U. A. Paulus, G. J. Feldmeyer, T. J. Schmidt, H. A. Gasteiger and R. J. Behm, *J. of New Mat. for Electrochem. Sys.*, 2000, **3**, 199.
33. W. Vogel, P. Britz, H. Bonnemann, J. Rothe and J. Hormes, *J. Phys. Chem. B*, 1997, **101**, 11029.
34. D. R. M. Godoi, J. Perez and H. M. Villullas, *J. Electrochem. Soc.*, 2007, **154**, B474.
35. J. F. Anderson, M. Kuhn, U. Diebold, K. Shaw, P. Stoyanov and D. Lind, *Physical Review B-Condensed Matter*, 1997, **56**, 9902.
36. K. D. Beard, M. T. Schaal, J. W. Van Zee and J. R. Monnier, *Appl. Catal. B*, 2007, **72**, 262.
37. M. T. Schaal, A. C. Pickerell, C. T. Williams and J. R. Monnier, *J. Catal.*, 2008, **254**, 131.
38. K. D. Beard, J. W. Van Zee and J. R. Monnier, *Appl. Catal. B*, 2009, **88**, 185.
39. M. Ohashi, K. D. Beard, S. Ma, D. A. Blom, J. St-Pierre, J. W. Van Zee and J. R. Monnier, *Electrochim. Acta*, 2010, **55**, 7376.
40. J. Rebelli, A. A. Rodriguez, S. Ma, C. T. Williams and J. R. Monnier, *Catal. Today*, 2011, **160**, 170.
41. J. Rebelli, M. Detwiler, S. G. Ma, C. T. Williams and J. R. Monnier, *J. Catal.*, 2010, **270**, 224.
42. Y.-J. Song, J. R. Monnier, P. T. Fanson and C. T. Williams, *J. Catal.*, 2014, **315**, 59.
43. S. S. Djokic, in *Modern Aspects of Electrochemistry*, eds. B. E. Conway and R. E. White, Springer, New York, NY, 2002, vol. 35, pp. 51.
44. K. D. Beard, D. Borelli, A. M. Cramer, D. Blom, J. W. Van Zee and J. R. Monnier, *ACS Nano*, 2009, **3**, 2841.
45. M. T. Schaal, A. Y. Metcalf, J. H. Montoya, J. P. Wilkinson, C. C. Stork, C. T. Williams and J. R. Monnier, *Catal. Today*, 2007, **123**, 142.
46. T. R. Garrick, W. Diao, J. M. Tengco, J. R. Monnier and J. W. Weidner, *ECS Trans.*, 2013, **53**, 79.
47. B. L. Garcia, B. Captain, R. D. Adams, A. B. Hungria, P. A. Midgley, S. J. M. Thomas and J. W. Weidner, *J. Clust. Sci.*, 2007, **18**, 121.
48. P. G. Corradini, F. I. Pires, V. A. Paganin, J. Perez and E. Antolini, *J. Nanopart. Res.*, 2012, **14**, 1080.
49. S. A. Tenney, B. A. Cagg, M. S. Levine, W. He, K. Manandhar and D. A. Chen, *Surf. Sci.*, 2012, **606**, 1233.
50. A. Illingworth, J. Zhou, O. Ozturk and D. A. Chen, *J. Vac. Sci. Technol. B*, 2004, **22**, 2552.
51. R. M. Nielsen, S. Murphy, C. Strebel, M. Johansson, J. H. Nielsen and I. Chorkendorff, *Surf. Sci.*, 2009, **603**, 3420.
52. R. P. Galhenage, S. C. Ammal, H. Yan, A. Duke, S. A. Tenney, A. Heyden and D. A. Chen, *J. Phys. Chem. C*, 2012, **116**, 24616.
53. M. T. Schaal, Ph. D. Thesis, University of South Carolina, 2009.
54. J. B. Park, S. F. Conner and D. A. Chen, *J. Phys. Chem. C*, 2008, **112**, 5490.

55. D. A. Chen, M. C. Bartelt, K. F. McCarty and R. Q. Hwang, *Surf. Sci.*, 2000, **450**, 78.
56. S. Stempel, M. Bäumer and H. J. Freund, *Surf. Sci.*, 1998, **404**, 424.
57. S. A. Tenney, W. He, C. C. Roberts, J. S. Ratliff, S. I. Shah, G. S. Shafai, V. Turkowski, T. S. Rahman and D. A. Chen, *J. Phys. Chem. C*, 2011, **115**, 11112.
58. J. S. Ratliff, Ph.D. Thesis, University of South Carolina, 2009.
59. F. Atamny and A. Baiker, *Appl. Catal. A*, 1998, **173**, 201.
60. L. L. Wang, X. C. Ma, Y. Qi, P. Jiang, J. F. Jia, Q. K. Xue, J. Jiao and X. H. Bao, *Ultramicroscopy*, 2005, **105**, 1.
61. A. R. Howells, L. Hung, G. S. Chottiner and D. A. Scherson, *Solid State Ionics*, 2002, **150**, 53.
62. K. A. Friedrich, F. Henglein, U. Stimming and W. Unkauf, *Electrochim. Acta*, 2000, **45**, 3283.
63. A. V. Kalinkin, A. M. Sorokin, M. Y. Smirnov and V. I. Bukhtiyarov, *Kinet. Catal.*, 2014, **55**, 354.
64. Y. X. Yao, Q. Fu, Z. Zhang, H. Zhang, T. Ma, D. Tan and X. H. Bao, *Appl. Surf. Sci.*, 2008, **254**, 3808.
65. I. N. Kholmanov, L. Gavioli, M. Fanetti, M. Casella, C. Cepek, C. Mattevi and M. Sancrotti, *Surf. Sci.*, 2007, **601**, 188.
66. W. R. Tyson and W. A. Miller, *Surf. Sci.*, 1977, **62**, 267.
67. C. D. Wagner, W. M. Riggs, L. E. Davis and J. F. Moulder, *Handbook of X-Ray Photoelectron Spectroscopy*, Perkin Elmer Corporation, Eden Prairie, MN, 1978.
68. H. Zhang, Q. Fu, Y. X. Yao, Z. Zhang, T. Ma, D. L. Tan and X. H. Bao, *Langmuir*, 2008, **24**, 10874.
69. I. Lopez-Salido, D. C. Lim and Y. D. Kim, *Surf. Sci.*, 2005, **588**, 6.
70. J. Z. Gao and Q. M. Guo, *Appl. Surf. Sci.*, 2012, **258**, 5412.
71. K. A. Wepasnick, X. Li, T. Mangler, S. Noessner, C. Wolke, M. Grossmann, G. Gantefoer, D. H. Fairbrother and K. H. Bowen, *J. Phys. Chem. C*, 2011, **115**, 12299.
72. Z. Song, T. H. Cai, J. C. Hanson, J. A. Rodriguez and J. Hrbek, *J. Am. Chem. Soc.*, 2004, **126**, 8576.
73. S. A. Tenney, J. S. Ratliff, W. He, C. C. Roberts, S. C. Ammal, A. Heyden and D. A. Chen, *J. Phys. Chem. C*, 2010, **114**, 21652.
74. J. B. Park, J. S. Ratliff, S. Ma and D. A. Chen, *Surf. Sci.*, 2006, **600**, 2913.
75. R. P. Galhenage, H. Yan, A. S. Ahsen, O. Ozturk and D. A. Chen, *J. Phys. Chem. C*, 2014, **118**, 17773.
76. E. M. Fiordaliso, S. Dahl and I. Chorkendorff, *J. Phys. Chem. C*, 2011, **115**, 25351.
77. A. Guttler, T. Zecho and J. Kuppers, *Surf. Sci.*, 2004, **570**, 218.